RSC Advances

PAPER

View Article Online
View Journal | View Issue

Check for updates

Cite this: *RSC Adv.*, 2025, **15**, 31272

Isoniazid–rhodanine molecular hybrids: design, synthesis, antimycobacterial activity and computational validation

Gobind Kumar,[a] Sahil Mishra,[a] Pule Seboletswe,[a] Neha Manhas,[a] Safiyah Ghumran,[a] Françoise Roquet-Banères,[b] Laurent Kremer,[bc] Gaurav Bhargava[d] and Parvesh Singh[a]

A novel series of isoniazid–rhodanine (INH–Rh) molecular hybrids (**9a–t**) was prepared and structurally characterized using different spectroscopic techniques, including FTIR, NMR (^{1}H, ^{13}C, HMBC, and HSQC), and HRMS. All the hybrids (**9a–t**), including their precursors (**3a–t** and **8a–t**), were assessed for their *in vitro* anti-tubercular activity, alongside the standard anti-tubercular drug, INH. Among them, **9d** (MIC = 1.56 μg ml^{-1}), **9j** (MIC = 12.50 μg ml^{-1}), and **9n** (MIC = 12.50 μg ml^{-1}) displayed the most potent activity against *M. tuberculosis (Mtb)*, with **9d** emerging as the most active. However, limited efficacy was observed for seven selected compounds (**3h**, **3i**, **9d**, **9j**, **9l**, **9n**, and **9p**) against INH-resistant *Mtb* strains harboring mutations in *KatG*. Moreover, the *Mtb* strain overexpressing the enoyl acyl carrier protein reductase (InhA) exhibited significant resistance to **9d**, **9j**, and **9n**, suggesting InhA as their likely target. Molecular docking studies revealed that the binding modes and key intermolecular interactions of the selected compounds closely resembled those of INH, a known inhibitor of InhA. ADME/T analysis indicated favorable pharmacokinetic and safety profiles for the synthesized compounds, while DFT calculations provided further insights into their global reactivity characteristics.

Received 23rd May 2025
Accepted 25th August 2025

DOI: 10.1039/d5ra03641k

rsc.li/rsc-advances

Open Access Article. Published on 01 September 2025. Downloaded on 2/11/2026 10:32:12 PM. This article is licensed under a Creative Commons Attribution-NonCommercial 3.0 Unported Licence.

1. Introduction

Tuberculosis (TB), an airborne infectious disease,[1] is caused by an obligate pathogen, *Mycobacterium tuberculosis (Mtb)*, which is responsible for ~1.4 million deaths every year.[2–4] According to the World Health Organization (WHO) report, in 2021, 10.6 million people were diagnosed with TB, resulting in approximately 1.6 million deaths, including 187 000 individuals living with HIV.[5] The high prevalence of TB in immunocompromised individuals, particularly those infected with HIV, underscores its significant global health impact.[6–9]

The current challenges for the treatment approach for TB involve a combination therapy of four primary drugs: pyrazinamide, isoniazid (INH), rifampin, and ethambutol, which are administered over 6 to 9 months.[10] The prolonged treatment regimen often leads to adverse side effects and low patient adherence, which contributes to the rise of multidrug-resistant TB (MDR-TB) and extensively drug-resistant TB (XDR-TB) strains.[11–13] The emergence of these resistant strains, along with the challenges posed by totally drug-resistant TB (TDR-TB) and co-infection with HIV, has made the control, diagnosis, treatment, and prevention of TB exceedingly lengthy and complicated.[14] The compounding of the various factors mentioned previously has resulted in TB becoming a serious global challenge that also imposes a significant economic burden on the countries most heavily impacted by the disease.[15] Thus, the development of novel anti-TB agents with distinct mechanisms of action and a low risk of cross-resistance with existing drugs is imperative. Despite extensive ongoing research, only a limited number of new anti-TB drugs have been successfully developed to date.[16]

The cell wall of *Mtb* is essential for its survival and pathogenicity,[17] as it provides structural support and protection.[18] It is composed of a complex, multi-layered network that includes mycolic acids, a highly branched arabinogalactan, and a cross-linked peptidoglycan matrix.[19,20] As the primary interface between the host and the pathogen, the *Mtb* cell wall represents a critical target for the design of new therapeutic inhibitors.[21] This includes first-line drugs such as INH,[22] which targets mycolic acid synthesis, and ethambutol,[23] which inhibits arabinogalactan biosynthesis in *Mtb*. However, the current treatment regimen faces several challenges, including drug toxicity, drug–drug interactions, high costs, and prolonged treatment

[a]*School of Chemistry and Physics, University of KwaZulu-Natal, P/Bag X54001, Westville, Durban 4000, South Africa. E-mail: singhp4@ukzn.ac.za*

[b]*Centre National de la Recherche Scientifique UMR 9004, Institut de Recherche en Infectiologie de Montpellier (IRIM), Université de Montpellier, 1919 route de Mende, 34293, Montpellier, France. E-mail: laurent.kremer@irim.cnrs.fr*

[c]*INSERM, IRIM, 34293 Montpellier, France*

[d]*Department of Chemical Sciences, I. K. Gujral Punjab Technical University, Kapurthala, Punjab-144603, India*

© 2025 The Author(s). Published by the Royal Society of Chemistry

Open Access Article. Published on 01 September 2025. Downloaded on 2/11/2026 10:32:12 PM. This article is licensed under a Creative Commons Attribution-NonCommercial 3.0 Unported Licence.

durations, all of which contribute to poor patient compliance.[24] In response to the growing threat of MDR strains, medicinal chemists must actively pursue the development of new and more effective drug candidates.

Thiazolidine analogs, especially rhodanine (Rh), have garnered considerable attention due to their diverse pharmacological activities, including anticancer,[25] anti-microbial,[26] anti-viral,[27] anti-malarial,[28] anti-diabetic,[29] and anti-TB properties.[30] Numerous Rh-based hybrids have been documented as anti-TB agents in the literature, with several potent compounds summarized along with their MIC or IC_{50} values in Fig. 1.[30–37] These compounds have also been reported to act as inhibitors of zinc metalloprotease 1 (Zmp1),[38,39] including derivatives such as ZTB19, ZTB20, and ZTB23 (ref. 40) and thyroid hormone receptor.[41–43] Furthermore, Rh-based derivatives have shown inhibitory activity against various key enzymes and biological targets, including 15-hydroxyprostaglandin dehydrogenase (15-PGDH),[44] aldose reductase,[45] HIV-1,[46] tyrosine kinases,[47] HCV protease, β-lactamase, JNK-stimulating phosphatase-1 (JSP-1), and PMT1 mannosyl transferase.[44]

On the other hand, INH is one of the best first-line prodrugs for the treatment of TB, which acts by blocking the NADH-dependent enoyl-acyl carrier protein reductase (InhA).[48] This enzyme participates in mycolic acid production during the elongation of the fatty acid chains.[49] Cessation of mycolic acid biogenesis brought on by InhA inhibition results in bacterial death.[50] INH is a prodrug that needs to be activated by the catalase/peroxidase KatG.[51] The prodrug's activation is decreased by mutations in the *katG* gene, lowering INH's efficacy.[52] As a result, creating substances that block InhA without requiring KatG activation may be an excellent way to create novel anti-TB medications.[53]

The concept of molecular hybridization (MH) has garnered significant global interest among synthetic and medicinal chemists in the realms of drug design and drug discovery.[54–59] This strategy involves the integration of two or more biologically active pharmacophores in a single molecular architecture, taking into account various chemical variables.[60] The primary goal of MH is to increase the efficacy, selectivity, and safety of the resulting molecular conjugates by integrating the beneficial properties of the parent molecules while simultaneously minimizing their potential side effects.[61,62]

Accordingly, various INH hybrids have been prepared by various researchers and assessed for their potency against *Mtb* and its drug-resistant strains (Fig. 1).[63–65]

In this work, we have developed a straightforward synthetic protocol to prepare a new series of INH–Rh molecular hybrids (**9a–t**) by coupling INH with rhodanine nuclei in a single unit.

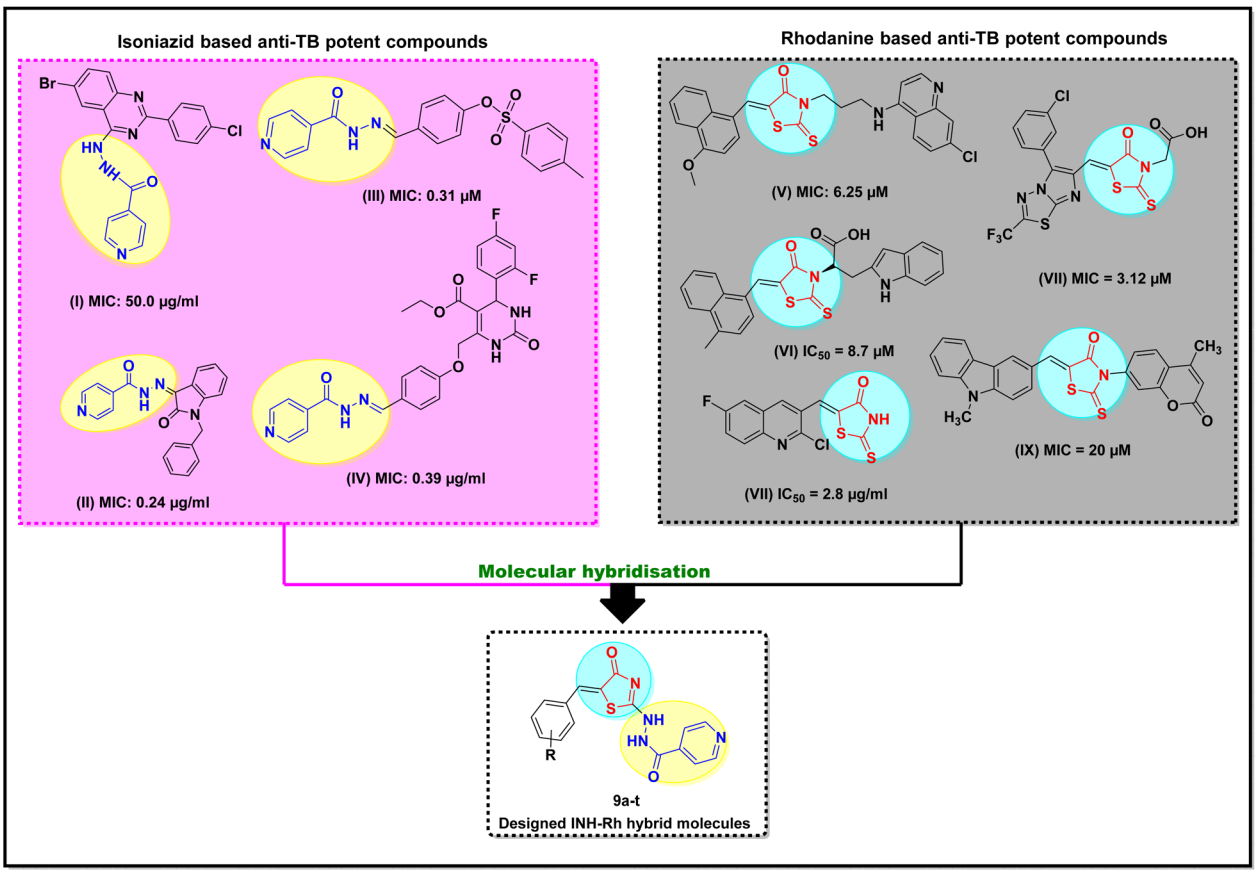

Fig. 1 Design and rationalization of INH–Rh molecular hybrids derived from isoniazid (INH) and rhodanine analogs *via* a molecular hybridization strategy.[32–34,66] MIC refers to the lowest concentration of an antimicrobial agent that prevents visible growth of a microorganism *in vitro* after a specified incubation period. IC_{50} refers to the concentration of a substance needed to inhibit a target by 50% in an *in vitro* assay.

Open Access Article. Published on 01 September 2025. Downloaded on 2/11/2026 10:32:12 PM. This article is licensed under a Creative Commons Attribution-NonCommercial 3.0 Unported Licence.

All synthesized compounds were structurally characterized through various spectroscopic techniques and evaluated for their activity against *Mtb.* The most potent compounds of the series were further tested against three INH-resistant strains of *Mtb*, followed by their cytotoxicity evaluation against the THP-1 cell line. Molecular docking studies were conducted to investigate the binding orientation and interaction profiles of representative compounds within the active site of InhA, a key enzyme involved in mycolic acid biosynthesis in *Mtb*. These simulations helped elucidate the host–guest relationship by identifying critical hydrogen bonding and hydrophobic interactions responsible for ligand stabilization within the binding pocket. Furthermore, *in silico* ADME/T (Absorption, Distribution, Metabolism, Excretion, and Toxicity) profiling revealed that the designed compounds exhibit favorable pharmacokinetic properties and comply with Lipinski's rule of five, suggesting good oral bioavailability and drug-likeness. To complement the docking studies, Density Functional Theory (DFT) calculations were performed to analyze the electronic properties of the most active compounds. Specifically, the energies of the frontier molecular orbitals (HOMO and LUMO), energy gaps, and global reactivity descriptors were evaluated, providing insights into the chemical stability and reactivity of the molecules.

2. Result and discussion

2.1. Chemistry

The synthetic protocols for the preparation of Intermediates I, II, III, and the final target compounds are outlined in Schemes 1A and 1B, and **2**. Initially, 5-benzylidene-2-thioxothiazolidin-4-ones (**3a–t**) were prepared using a reported method,[67] which involves the condensation of substituted aromatic aldehydes (**1a–t**, 1 eq.) with rhodanine (2, 1 eq.) in the presence of sodium acetate (1 eq.) and acetic acid, as depicted in Scheme 1A. The synthesis of the initially designed molecular hybrid (7) was executed in two steps, as outlined in Scheme 1. In the first step, compound **3a** (1 eq.) was reacted with ethyl bromoacetate (1.5 eq.) (**4**) in the presence of K_2CO_3 (2.5 eq.) and DMF to offer intermediate **5**, albeit in low yield. In the second step, this crude product was refluxed with INH (6, 1 eq.) in ethanol to afford the final compound (Scheme 1B). However, the absence of a characteristic $-CH_2$ peak in the ^{1}H NMR spectrum suggested that compound (**9**), and not the expected hybrid **7**, was formed. This observation further implied that compound **8**, rather than **5**, was the actual intermediate generated in step 1. Subsequently, nucleophilic attack by the amine group of INH amine likely resulted in the elimination of the mercapto ethyl ester moiety, leading to the formation of compound **9a** (Scheme 1B).

Considering the slow reaction rate of step 1 coupled with the low yield (34%) of intermediate **8**, we decided to place a better leaving group on **3** for *S*-alkylation before engaging it in nucleophilic aromatic substitution reaction with INH. For this purpose, first, we reacted **3a** with methyl iodide using triethylamine as a base in DCM. The corresponding *S*-methylation proceeded smoothly, offering the desired product **8a** in a much better yield (90%). Following the same protocol, other analogues (**8b–t**) were prepared in good yields (84–96%) before subjecting them to their hybridization with INH in ethanol to offer their INH–Rh molecular hybrids (**9a–t**) in good yields (86–97%) (Scheme 2). All INH–Rh derivatives (**9a–t**) and their corresponding intermediates (**8a–t**) are structurally illustrated in Schemes S1 and S2 of the Supplementary Information.

2.2. Structural elucidation

Different spectroscopic techniques, such as ^{1}H-NMR, ^{13}C-NMR, infrared radiation (IR), and high-resolution mass spectrometry (HRMS), were utilized to characterize the structures of all the molecular hybrids (**9a–t**). The corresponding spectral data are presented in the SI. Additionally, two-dimensional (2D) NMR data (HSQC and HMBC) were used to facilitate complete structural assignment of the representative compound **9b**.

For example, the IR spectrum of **9b** (Fig. S49) showed three characteristic absorbances at ν 1712 cm^{-1} and 1650 cm^{-1} accounting for the two carbonyl groups as well as a broad peak at 1600 cm^{-1} representing benzylidene double bond (C=C). In its ^{1}H NMR spectrum (Fig. S50), the INH moiety displayed two NH protons, NH-14 and NH-15, resonating as two broad singlet peaks far downfield at δ_H 11.42 and 12.60 ppm, respectively. A characteristic singlet at δ_H 7.63 ppm for the CH-6 proton confirmed the condensation of rhodanine with the aldehyde (C=C–H) moiety. Furthermore, as expected, the methyl group (H-13) appeared as the most upfield resonance at δ_H 2.33 ppm. The rhodanine ring carbons C-3 and C-5 appeared at 167.99 and 150.77 ppm, respectively, in its ^{13}C spectrum (Fig. S51), along with the most upfield signal at 21.50 ppm corresponding to C-13. The INH moiety's carbonyl carbon (C-16) displayed the second most downfield resonance at 162.66 ppm. Finally, the HRMS spectrum of compound **9b** (Fig. S52) exhibited a molecular ion peak of *m*/*z* 337.0759 and further confirmed the assigned structure.

The necessary carbons of the representative compound (**9b**) were successfully determined by heteronuclear multiple bond coherence (HMBC) data. For example, the INH proton H-18 (δ_H 8.77 ppm) showed HMBC correlations with C-16 (δ_C 162.66), C-17 (δ_C 140.62), C-19 (δ_C 121.92), and C-22 (δ_C 150.60) (Fig. 2). Rhodanine proton H-6 (δ_H 7.21 ppm) showed HMBC correlations with C-5 (δ_C 167.99), C-1 (δ_C 121.57), and C-7 (δ_C 130.92), while the aldehyde ring proton H-11 (δ_H 7.29 ppm) displayed correlations with C-7 (δ_C 130.92), C-10 (δ_C 140.51), and C-13 (δ_C 21.50). The proton H-13 showed HMBC correlation with carbon C-9 (δ_C 130.31) and C-10 (δ_C 140.51).

2.3. Biological studies

2.3.1. *In vitro* activity against wild-type *M. tuberculosis*.

All INH–Rh molecular hybrids (**9a–t**), their precursors (**3a–t** and **8a–t**), and INH (as the control drug), were tested against *Mtb* $mc^2$6230 to assess their anti-TB activity. The results are depicted in Table 1. Experiments were conducted three times independently with similar values.

The MIC values of the benzylidene series (**3a–t**) span between 25 to 200 μg ml^{-1}. The two most active compounds (**3h** and **3i**) of this series displayed the lowest MIC value (25 μg ml^{-1}),

 © 2025 The Author(s). Published by the Royal Society of Chemistry

Open Access Article. Published on 01 September 2025. Downloaded on 2/11/2026 10:32:12 PM.
This article is licensed under a Creative Commons Attribution-NonCommercial 3.0 Unported Licence.

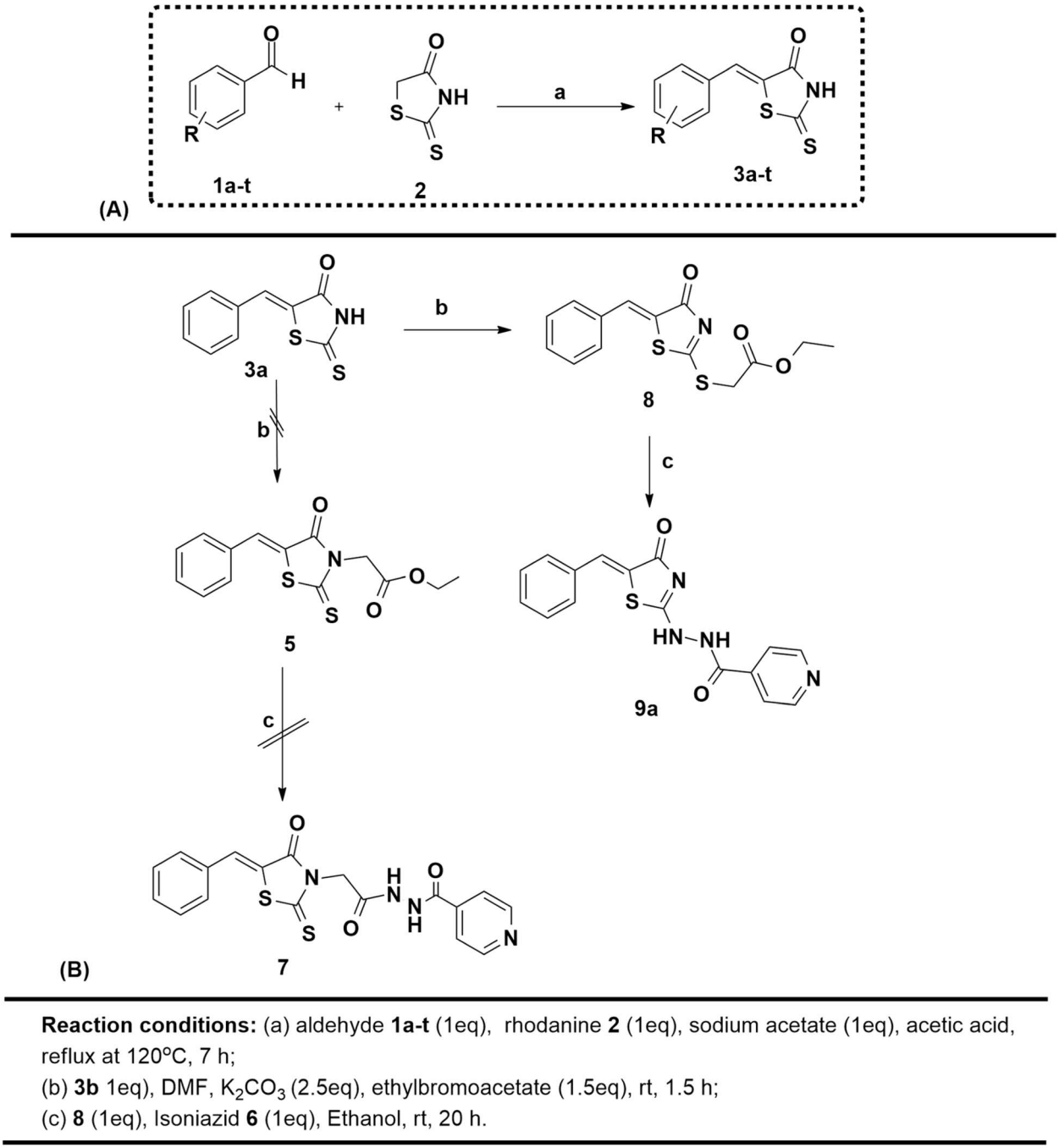

Scheme 1 (A) Illustrates the synthesis of **3a–t**. (B) Illustrates the synthesis of 4,5-dihydrothiazole-2-thiol.

whereas the compound **3f** (MIC = 200 μg ml^{-1}) exhibited the least inhibitory activity. Most of the other tested compounds (except **3h**, **3i**, and **3f**) exhibited MIC values between 50 and 100 μg ml^{-1}, demonstrating low anti-TB activity of this series of compounds.

The thiomethyl analogues (**8a–t**), used as intermediates in the final step, generally displayed lower activity compared to their precursors (**3a–t**), with most compounds showing MIC values in the range of 100–200 μg ml^{-1}. Notably, only compound **8q** showed moderate activity with an MIC of 50 μg ml^{-1}. These findings indicate a marked reduction in activity following *S*-methylation of the thiocarbonyl group.

As anticipated, the INH–Rh molecular hybrids (**9a–t**) exhibited relatively improved activity profiles than their synthetic precursors (**3a–t**, **8a–t**), with MIC values ranging from 1.56 to 100 μg ml^{-1}. The molecular hybrid **9d** emerged as the most active compound with an MIC of 1.56 μg ml^{-1}. The molecular hybrids **9j** and **9n**, which were the second most active compounds in the series, inhibited the bacterial growth at a concentration of 12.50 μg ml^{-1}. Other compounds, such as **9f**,

Open Access Article. Published on 01 September 2025. Downloaded on 2/11/2026 10:32:12 PM.
This article is licensed under a Creative Commons Attribution-NonCommercial 3.0 Unported Licence.

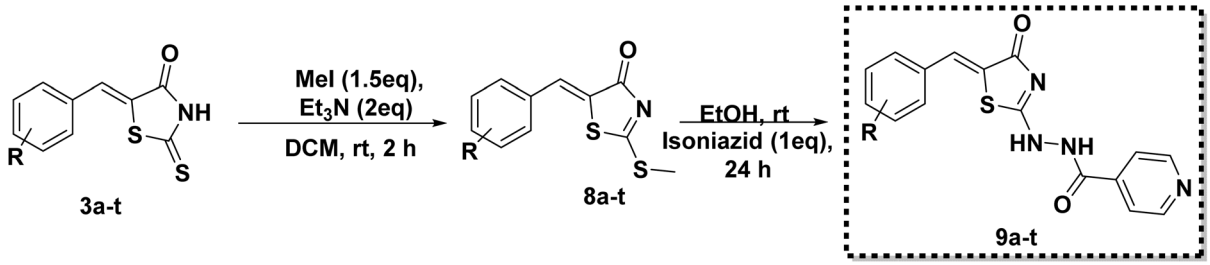

(9a) R= H
(9b) R= 4-Me
(9c) R= 3-Me
(9d) R= 2-Me
(9e) R= 4-OMe
(9f) R= 2-OMe
(9g) R= 3,4,5-triOMe
(9h) R= *i*-Propyl
(9i) R= Cinnamal
(9j) R= 4-F
(9k) R= 3-F
(9l) R= 2-F
(9m) R=2,4-diF
(9n) R= 4-Cl
(9o) R= 3-Cl
(9p) R= 2-Cl
(9q) R= 2,4-diCl
(9r) R= 4-Br
(9s) R= 3-Br
(9t) R= 2-Br

Scheme 2 Synthesis of final INH–Rh molecular hybrids.

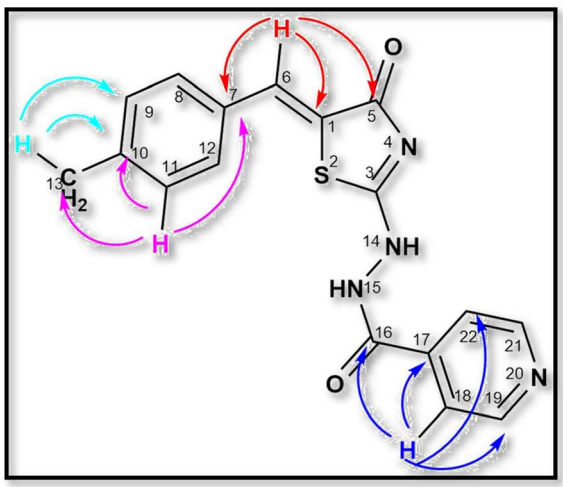

Fig. 2 Schematic representation of key HMBC correlations in compound **9b**.

9k, **9l**, and **9p** displayed moderate inhibition (MIC = 25 μg ml^{-1}). The remaining compounds of the series exhibited relatively higher MIC values ranging from 50 to 100 μg ml^{-1}.

2.3.2. Structure–activity relationship analysis. The structure–activity relationship (SAR) of the tested INH–Rh molecular hybrids established in terms of different bioisosteres is described in Table 1. For instance, compound **9a** without any substituent on the phenyl ring demonstrated moderate activity (MIC = 50 μg ml^{-1}) against *Mtb*. The substitution of a methyl group at the *ortho* position dramatically improved the activity of **9d** (MIC = 1.56 μg ml^{-1}). However, the placement of the same methyl group at *para* (**9b**, MIC = 50 μg ml^{-1}) or *meta* (**9c**, MIC = 50 μg ml^{-1}) positions reduced the activity by ~32-fold. A similar trend was observed for the methoxy-substituted analogues, where *ortho*-substitution (**9f**, MIC = 25 μg ml^{-1}) conferred fourfold higher activity compared to *para*-substitution (**9e**, MIC = 100 μg ml^{-1}). The presence of multiple methoxy groups at (**9g**) or a bulkier isopropyl group at the *para* position (**9h**) was detrimental to the activity (MIC = 100 μg ml^{-1}). These results indicate that the placement of electron-donating groups at the *ortho* position of the phenyl ring is beneficial to the activity of the hybrids. Their halogenated analogues, however, presented the opposite trend, where the *para*-fluoro analogue (**9j**, MIC = 12.50 μg ml^{-1}) was found to be ~2-fold more active than its *meta* (**9k**) and *ortho* (**9l**) counterparts. Similarly, the chlorine, when positioned at the *para* (**9n**, MIC = 12.50 μg ml^{-1}) position, offered a more potent compound than its *meta* (**9o**, MIC = 50 μg ml^{-1}) or *ortho* (**9p**, MIC = 25 μg ml^{-1}) analogues. Like **9g**, the placement of multiple fluorine (**9m**) or chlorine (**9q**) atoms on the phenyl ring decreased the activity (MIC = 100 μg ml^{-1}). The *para* and *ortho* bromo analogues (**9r**, MIC = 50 μg ml^{-1} and **9t**, MIC = 50 μg ml^{-1}) presented superior activity to their *meta*-substituted analogue (**9s**, MIC = 100 μg ml^{-1}). However, all compounds were less active than INH (MIC = 0.039 μg ml^{-1}), suggesting that further structural modifications are needed to enhance their activity. A brief schematic illustration of SAR is presented in Fig. 3.

2.3.3. *In vitro* activity against *Mtb* KatG mutants. We selected seven active hybrid compounds (**3h**, **3i**, **9d**, **9j**, **9l**, **9n**, and **9p**) to evaluate them further against three INH-resistant *Mtb* strains harboring mutations in the catalase-peroxidase *katG* gene (mc^{2}6230_R1, mc^{2}6230_R2, mc^{2}6230_R3), and the results are presented in Table 2.

Like INH, all tested compounds (except for **3h** and **3i**) lost their activity against the three KatG mutants. For instance, **9d**'s MIC escalated from 1.56 μg ml^{-1} in the parental strain to 50 μg ml^{-1} (32-fold increase) in the mutated strains. Similarly, compounds **9j** (8-fold), **9l** (4-fold), **9n** (8-fold), and **9p** (4-fold) displayed significant loss of their activity against the mutants. These results suggest that most of the hybrids require KatG-dependent activation to exert their action.

To confirm that the compounds share the same mechanism of action as INH by blocking InhA, we tested the three more active compounds (**9d**, **9j**, and **9n**) against the *Mtb* mc^{2}6230

© 2025 The Author(s). Published by the Royal Society of Chemistry

Open Access Article. Published on 01 September 2025. Downloaded on 2/11/2026 10:32:12 PM. This article is licensed under a Creative Commons Attribution-NonCommercial 3.0 Unported Licence.

Table 1 Antitubercular evaluation of series **3a–t**, **8a–t**, and **9a–t** against *Mtb* mc^{2}6230

Product code	MIC[a] (μg ml^{-1})	Product code	MIC[a] (μg ml^{-1})	Product code	MIC[a] (μg ml^{-1})
3a	50	**8a**	100	**9a**	50
3b	50	**8b**	100	**9b**	50
3c	100	**8c**	100	**9c**	50
3d	50	**8d**	200	**9d**	**1.56**
3e	100	**8e**	100	**9e**	100
3f	200	**8f**	50	**9f**	25
3g	50	**8g**	100	**9g**	100
3h	25	**8h**	100	**9h**	100
3i	25	**8i**	100	**9i**	50
3j	50	**8j**	100	**9j**	**12.5**
3k	50	**8k**	100	**9k**	25
3l	100	**8l**	100	**9l**	25
3m	50	**8m**	100	**9m**	100
3n	50	**8n**	100	**9n**	**12.5**
3o	50	**8o**	200	**9o**	50
3p	100	**8p**	100	**9p**	25
3q	100	**8q**	50	**9q**	100
3r	50	**8r**	100	**9r**	50
3s	50	**8s**	200	**9s**	100
3t	100	**8t**	100	**9t**	50
INH[b]	0.039				

[a] MIC_{99} = minimum inhibitory concentration that inhibits 99% of bacterial growth (μg ml^{-1}). [b] INH = isoniazid (standard drug).

strain overexpressing InhA, under the strong constitutive *hsp60* promoter (Table 3).

The overexpression of InhA leads to high levels of resistance to each inhibitor (4 to 16-fold) increase compared to the control strain harboring the empty pMV261, similar to INH (16-fold increase in MIC), which suggests that these hybrid compounds inhibit InhA. As expected, the efficacy of RIF, an RNA polymerase inhibitor, was unaffected in the InhA-overexpressing strain. Together, these results indicate that the hybrids behave similarly to INH by requiring a bioactivation step catalyzed by KatG, and inhibiting InhA activity, presumably by forming adducts with NAD, as previously shown with INH.[68]

2.3.4. *In vitro* cytotoxicity studies. Many anti-TB drugs exhibit toxicity toward eukaryotic cells, prompting us to evaluate the potential cytotoxic effect of the molecular hybrids **9d**, **9j**, **3h**, and **3i** in human THP-1 cells. The cells were incubated at 37 °C and 5% CO_2 for either 24 h (D1, left panel) or 72 h (D3, right panel) (Fig. 4). DMSO served as the negative control, while 10% SDS was used as the positive control (data not shown). INH was included as an internal control. The results indicate that

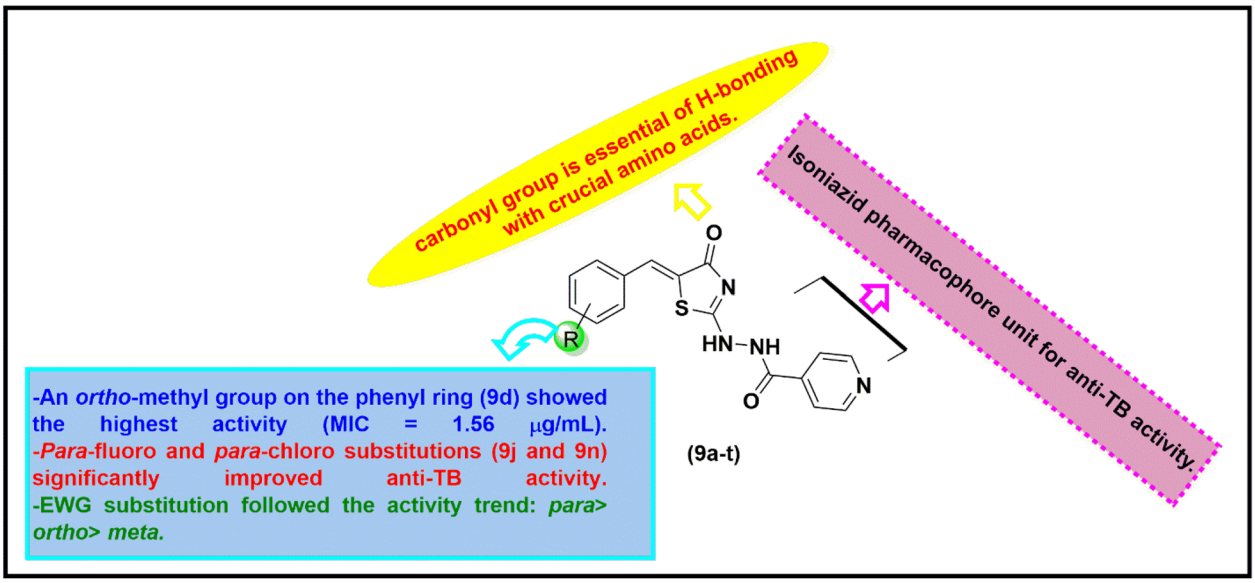

Fig. 3 Brief SAR summary compounds **9a–t**.

Open Access Article. Published on 01 September 2025. Downloaded on 2/11/2026 10:32:12 PM. This article is licensed under a Creative Commons Attribution-NonCommercial 3.0 Unported Licence.

Table 2 MIC of the most potent hybrid compounds against *Mtb* strains with mutations in KatG. Experiments were conducted three times independently with similar values

	MIC (μg ml^{-1})			
Product code	mc^{2}6230 (parental strain)	mc^{2}6230_R1	mc^{2}6230_R2	mc^{2}6230_R3
3h	25	25	25	25
3i	25	50	50	50
9d	1.56	50	50	50
9j	12.50	100	100	100
9l	25	100	100	100
9n	12.50	100	100	100
9p	25	100	100	100
INH	0.039	>10	>10	>10

Table 3 MICs of **9d**, **9j** and **9n** against mc^{2}6230 overexpressing InhA. Experiments were conducted three times independently with similar values

	MIC (μg ml^{-1})		
Compound	Wild-type	pMV261	pMV261_*inhA*
9d	1.56	3.12	50 (16)[a]
9j	12.5	12.5	100 (8)
9n	12.5	25	100 (4)
RIF	0.039	0.039	0.039 (1)
INH	0.078	0.078	1.25 (16)

[a] Indicates the fold change between the strain harboring the empty plasmid pMV261 and the strain overexpressing InhA.

the compounds tested exhibited IC_{50} values >15 μg ml^{-1} (Table 4), indicating cytotoxicity toward THP-1 cells at concentrations close to the MIC values, except **9d**, which displays a SI of 14, while INH displays a SI >100 under the same experimental conditions. Thus, the cytotoxicity profiles of the tested compounds appear essentially non-favorable as compared to INH.

2.4. Computational studies

2.4.1. Molecular docking. Molecular docking is a reliable tool in biological research to identify ligand–protein interactions. Here, *in silico* molecular docking was utilized to analyze the binding interactions of the most potent compounds with InhA from *Mtb* (PDB ID: 4QXM). We aimed to correlate the experimental activity trend with the computed docking score and explore their binding conformations. Based on the potency, compounds **9d**, **9j**, **9n**, and reference INH were chosen for Induced Fit Docking (IFD) studies, and their docked complexes showing different ligand–receptor interactions are presented in Fig. 5, while the results are summarized in Table 5.

Compound **9d** demonstrated the highest docking score of −7.454 among all potent compounds, suggesting its strong binding affinity to the target. It interacts with InhA through both hydrogen bonding and hydrophobic interactions. For instance, the N atom of the pyridine ring, the carbonyl oxygen of the rhodanine moiety, and the NH group of the INH fragment formed a network of hydrogen bonds with amino acid residues Arg43 (d = 2.17 Å), Met199 (d = 2.42 Å), Ala198 (d = 2.31 Å), and Gly96 (d = 1.86 Å), respectively. In addition, the aromatic ring engaged in a π–π stacking interaction with the Phe149 (d = 4.79

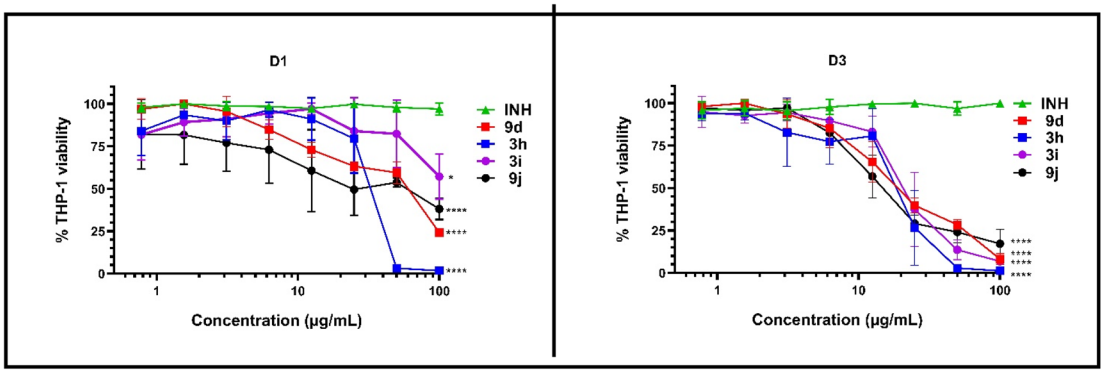

Fig. 4 Cytotoxicity assay of **9d**, **9j**, **3h**, and **3i** in THP-1 cells. Cells were differentiated with PMA for 48 h and exposed to increasing concentrations of each compound (starting at 100 μg ml^{-1}) for an additional 24 h (D1, left panel) or 72 h (D3, right panel) at 37 °C with 5% CO_2. INH was included as a reference drug. Data shown are the mean of two independent experiments completed in technical duplicates, with error bars representing the standard deviations. Statistical analysis was performed using ordinary one-way ANOVA between the lowest and highest concentrations used for all compounds. *: p < 0.05; ****: p < 0.0001.

© 2025 The Author(s). Published by the Royal Society of Chemistry

Open Access Article. Published on 01 September 2025. Downloaded on 2/11/2026 10:32:12 PM. This article is licensed under a Creative Commons Attribution-NonCommercial 3.0 Unported Licence.

Table 4 Selectivity index determined from cytotoxicity studies

Product code	MIC (μg ml^{-1})	IC_{50}[a] (μg ml^{-1})	SI[b]
3h	25	15	0.6
3i	25	22	0.9
9d	1.56	21	14
9j	12.50	18	1.4
INH	0.039	>100	>100

[a] IC_{50} represents the drug concentration that reduces the viability of THP-1 cells by 50%, determined after 72 h of exposure to the compounds (Fig. 4). [b] SI, selectivity index (IC_{50}/MIC).

Å) residue (Fig. 5). According to the reported documents, the hydrophobic interaction of Gly96 and Phe149 amino residues helps to enhance the stability of the ligand–enzyme complex, which in turn is considered very important in InhA inhibition.[69,70] Compound **9j** and **9n** displayed comparable docking scores of −6.681 and −6.661, respectively, suggesting similar binding affinities towards the InhA enzyme. However, their interaction modes differed notably. Compound **9j** formed hydrogen bonds with Gly96 (d = 2.24 Å) and Thr196 (d = 2.28 Å), along with a π–π stacking interaction with Phe149 residue (d = 5.24 Å) (Fig. S1). In contrast, **9n** displayed a single hydrogen bond interaction with Met98 (d = 2.47 Å) through the carbonyl group of the rhodanine ring (Fig. S2). The reference drug INH showed the highest docking score of −7.772 and displayed two hydrogen bond interactions with Thr162 (d = 2.03 Å) and a hydrophobic interaction with Phe149 (d = 4.13 Å).

2.4.2. ADME/T analysis. *In silico* studies offer a means to examine pharmacokinetic parameters such as Absorption, Distribution, Metabolism, Excretion, and Toxicity (ADME/T). The ADME studies on the most potent compounds, **9d**, **9j**, and **9n**, involved a comprehensive evaluation of various physicochemical parameters essential for assessing drug-likeness and pharmacokinetic properties.

Table 5 The molecular docking results of potent compounds **9d**, **9j**, and **9n**, along with INH

Product code	MIC (μg ml^{-1})	Docking score	Glide Emodel	Glide energy
9d	1.56	−7.454	−92.144	−60.488
9j	12.50	−6.681	−83.662	−54.384
9n	12.50	−6.661	−69.308	−49.613
INH	0.039	−7.772	−50.685	−34.360

2.4.2.1. Lipinski's rule and physicochemical properties. To verify the drug similarity properties based on Lipinski's rule and ADME-Tox characteristics, we utilized the QikProp and two online tools, SwissADME and pkCSM, for each proposed molecule. To enhance the readability of Fig. 6, the terms FLEX, INSATU, INSOLU, POLAR, SIZE, and LIPO: FLEX stands for flexibility (no more than nine rotatable bonds), INSATU signifies saturation (the value should be at least 0.25), INSOLU indicates solubility (log S should not exceed 6), POLAR represents polarity (topological polar surface area (TPSA) standard range 20 Å^2 to 140 Å^2), SIZE denotes molecular weight (standard range 150 to 500 g mol^{-1}), and LIPO refers to lipophilicity (standard range −0.7 and 5).[71] Accordingly, these compounds (**9d**, **9j**, and **9n**) showed a good compliance with all these parameters.

For good oral bioavailability, the MW, no. rot. Bond, HBD, HBA, TPSA, and QPlog $P_{o/w}$ are the key parameters demonstrating the oral bioavailability of molecules after administration and excretion through the kidney.[72] TPSA indicates how drug molecules are distributed throughout the body. Similarly, higher values of QPlog $P_{o/w}$ indicate a greater affinity for lipophilic environments, influencing bioavailability and potential for crossing biological membranes.[73] Table S1 illustrates that all compounds followed these criteria.

2.4.2.2. In silico rules, bioavailability score, and synthetic accessibility. Table S2 presents a comparative analysis of the

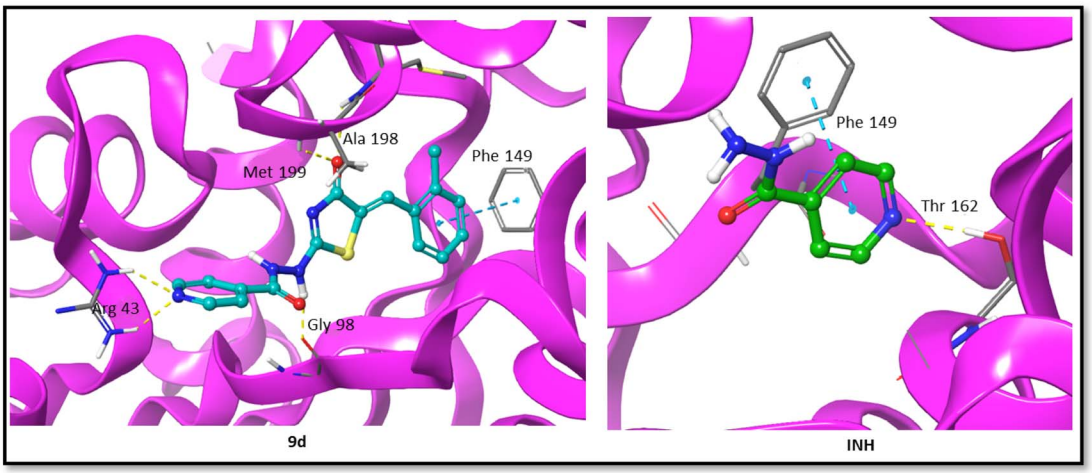

Fig. 5 3D representation of ligand–receptor interactions for compound **9d** and standard INH. The yellow color represents hydrogen bonding, and the blue color shows π–π interaction.

Open Access Article. Published on 01 September 2025. Downloaded on 2/11/2026 10:32:12 PM.
This article is licensed under a Creative Commons Attribution-NonCommercial 3.0 Unported Licence.

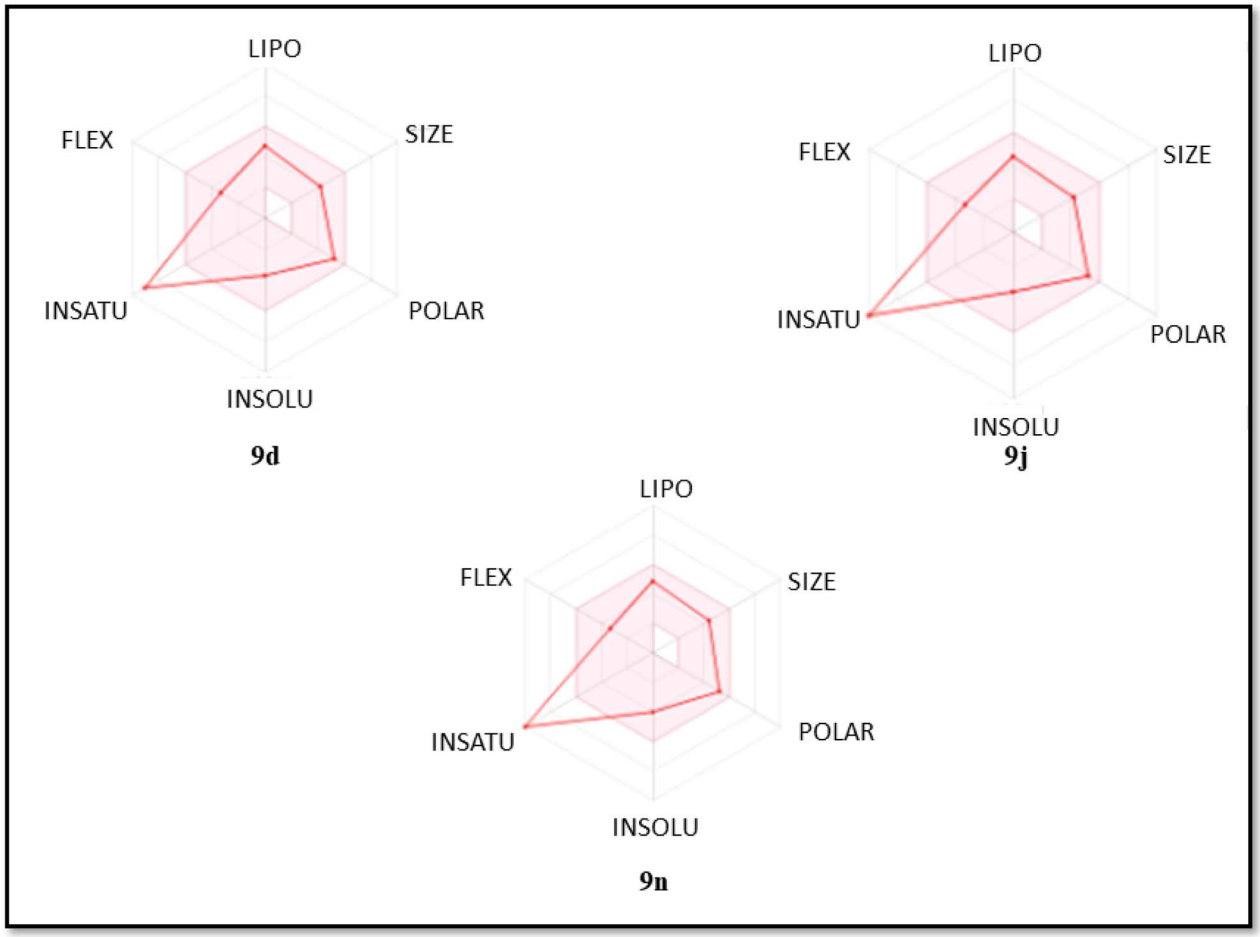

Fig. 6 The Radar diagrams of compounds **9d**, **9j**, and **9n**.

bioavailability and adherence to various *in silico* rules, such as Muegge, Ghose, Veber, and Egan, for the most active compounds **9d**, **9j**, and **9n**, which showed good compliance. The synthetic accessibility scores for all compounds were below 4,[74] indicating that they are readily synthesizable.

Table S3 explored the ADMET analysis using pkCSM, demonstrating pharmacokinetic and toxicity profiles for compounds **9d**, **9j**, and **9n**. Water solubility indicates how easily a compound dissolves in water, which is crucial for drug absorption and formulation. Typically, compounds with log mol l^{-1} values closer to 0 are considered well-soluble. Compounds **9d** and **9n**, with lower values, predicted their high solubility. Human intestinal absorption (HIA) indicates the percentage of the administered dose absorbed into the bloodstream from the intestines after oral administration.[75] The HIA percentage of more than 70% is considered a higher absorption ability of the drugs.[76] Results in Table S3 demonstrate that all compounds with more than 90% HIA value are generally preferred for better bioavailability. Compound **9d** demonstrates high intestinal absorption (94.19%), indicating efficient uptake.

Parameters such as QPlogBB, VDss, and CNS were evaluated computationally to analyze the distribution of compounds **9d**, **9j**, and **9n** in the body. QPlogBB, or Predicted Logarithm of the Blood–Brain Barrier (BBB) Partition Coefficient, plays a crucial role in drug development. For BBB permeability, the drug molecules with a logBB value >0.3 easily cross the BBB, while logBB value <−1 cannot cross the BBB. Table S3 demonstrates that compounds **9d**, **9j**, and **9n** were within the standard range.[77] VDss stands for volume distribution steady state; a higher VDss value indicates that the drugs are more distributed in the tissue than in the plasma. The VDss value is good for a drug if it is higher than 0.45.[78] The prediction results demonstrated that two compounds (**9d** and **9j**) meet these criteria. The central nervous system (CNS) permeability for the drug molecule with a standard log *PS* value [−2 (inactive) to +2 (active)] suggests that they are unable to cross the CNS.[79] Accordingly, **9d**, **9j**, and **9n** showed no CNS permeability.

Regarding the toxicity of the potent compound, the AMES and skin sensitization parameters were predicted. The AMES toxicity has demonstrated that the compound exhibits mutagenicity in the AMES test, which assesses the potential to cause genetic mutations.[80] Ideally, compounds should not exhibit AMES toxicity. Table S3 suggests that all compounds do not show any AMES toxicity. These individual evaluations emphasize how crucial it is to consider each molecule's distinctive

© 2025 The Author(s). Published by the Royal Society of Chemistry

Open Access Article. Published on 01 September 2025. Downloaded on 2/11/2026 10:32:12 PM.
This article is licensed under a Creative Commons Attribution-NonCommercial 3.0 Unported Licence.

qualities during the drug development and assessment process to ensure both safety and efficacy. Table S3 demonstrates that the potent compounds did not show any toxicity to the skin.

2.4.3. DFT studies. The Density Functional Theory (DFT) calculations were finally applied to explore the frontier molecular orbitals, global reactivity properties, and molecular potential energy[81,82] of the compounds **9d**, **9j**, and **9n**.

2.4.3.1. Structural optimization energy. First, the geometry of compounds **9d**, **9j**, and **9n** was optimized at the B3LYP level using the 6-31++G (d, p) basis sets.[83] The number and type of atoms in each compound are illustrated in Fig. 7, while their computed electronic energies and dipole moments are summarized in Table 6. The low electronic energies of these compounds indicate their strong tendency to form stable non-covalent interactions with the target enzyme, which may contribute to enhanced binding affinity and biological activity.

Similarly, compounds **9d**, **9j**, and **9n** exhibited dipole moments of 5.16, 4.60, and 4.62 Debye, respectively. These values suggest high aqueous solubility and may enhance membrane permeability, particularly in *Mtb*, which possesses a lipid-rich cell wall.

2.4.3.2. Frontier molecular orbital (FMO) analysis. Frontier Molecular Orbitals (FMO) studies were conducted to analyze E_{HOMO}, E_{LUMO}, and ΔE_{gap} (Table 7). The HOMO and LUMO energies are crucial to determining the reactivity and kinetic stability of the molecules,[84] with the negative values suggesting more stability.[85] For **9d**, **9j**, and **9n**, the respective computed HOMO energies were −5.13, −4.94, and −4.96 eV, while for LUMO energies for the same compounds were predicted to be −2.21, −2.31, and −2.23 eV.

Table 6 The structural optimized energy and dipole moment using DFT/B3LYP/6-31++G (d, p)

Product code	Dipole moment (Debye)	Electronic energy (Hartree)
9d	5.16	−1424.48
9j	4.60	−1484.41
9n	4.62	−1844.76

The HOMO with higher energy indicates a better ability of the compound to donate electrons (nucleophilic) to other biomolecules that have lower energy. Whereas the higher energy of LUMO indicates a better ability to accept electrons (electrophilic).[85]

The energy gap serves as a quantitative indicator of a compound's stability and reactivity.[86–88] A smaller energy gap between HOMO and LUMO suggests that the compound is less stable and more reactive, and *vice versa*.[89–91] Additionally, a small energy gap often indicates that the molecule is of significant biological potential.[92] Table 7 shows that compounds **9d** (2.92 eV), **9j** (2.62 eV), and **9n** (2.73 eV) possess a smaller energy gap, indicating higher reactivity and significant biological potential. Moreover, it is noted that when the frontier molecular orbitals (FMOs) are localized on the same side with lobes of identical phase (same colour), the compounds tend to display reduced biological activity.[93] As illustrated in Fig. 8, the FMOs of these compounds are distributed on opposite sides, where the green orbital represents regions of low electron density and the red orbital corresponds to regions of high electron density.[94] In addition, we calculated the global reactivity properties (Table S4) such as

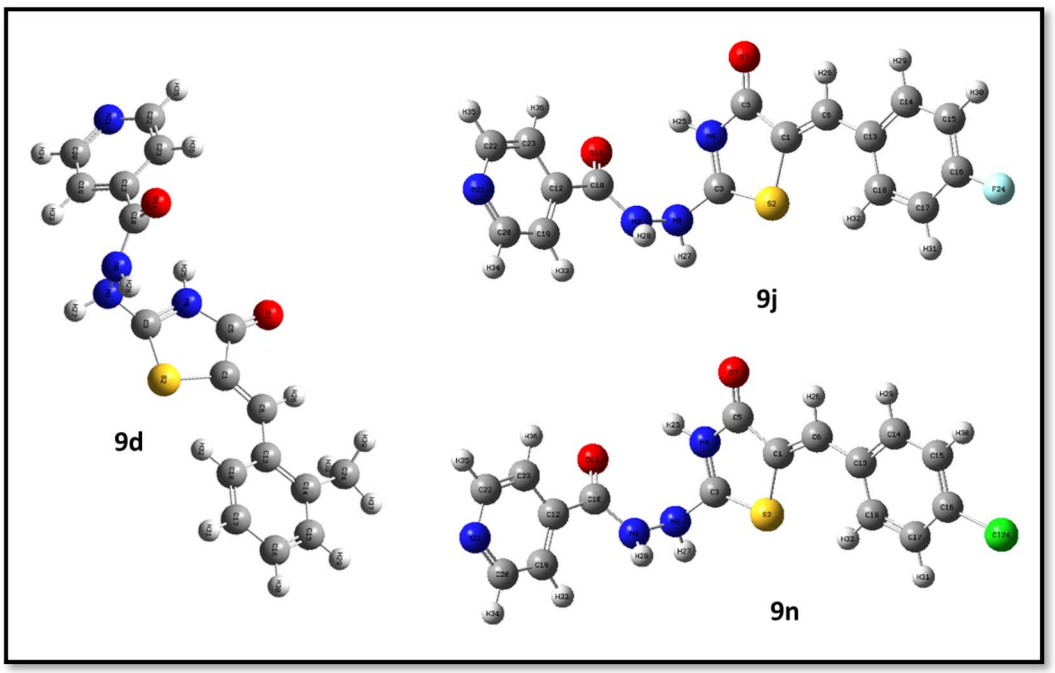

Fig. 7 Illustrate the optimized structure of the compounds **9d**, **9j**, and **9n** using DFT/B3LYP/6-31++G (d, p).

Open Access Article. Published on 01 September 2025. Downloaded on 2/11/2026 10:32:12 PM. This article is licensed under a Creative Commons Attribution-NonCommercial 3.0 Unported Licence.

Table 7 The FMOs analysis and calculated E_{HOMO}, E_{LUMO}, and ΔE values for potent compounds[a]

S. no.	Physical properties	9d	9j	9n
1	E_{HOMO} (eV)	−5.13	−4.94	−4.96
2	E_{LUMO} (eV)	−2.21	−2.31	−2.23
3	ΔE (eV)	2.92	2.62	2.73

[a] E_{HOMO} = energy of highest occupied molecular orbital; E_{LUMO} = energy of lowest unoccupied molecular orbital; ΔE = energy band gap between HOMO and LUMO.

ionization energy, electron affinity, electronegativity, chemical potential, softness, and hardness, and the results are provided in the SI along with their discussion. Moreover, molecular electrostatic potential surface analysis was also performed, and the results are provided in Fig. S3.

3. Conclusion

In this study, we successfully synthesized and evaluated a novel library of INH–Rh molecular hybrids (**9a–t**) for their anti-tubercular activity. Among these, compound **9d** demonstrated the highest potency, with a MIC of 1.56 μg ml^{-1}, highlighting the potential of INH–Rh hybridization in enhancing anti-TB efficacy. This hypothesis was further supported by molecular docking studies, which revealed that the active compounds adopt favorable binding orientations and form key intermolecular interactions within the InhA active site. While several

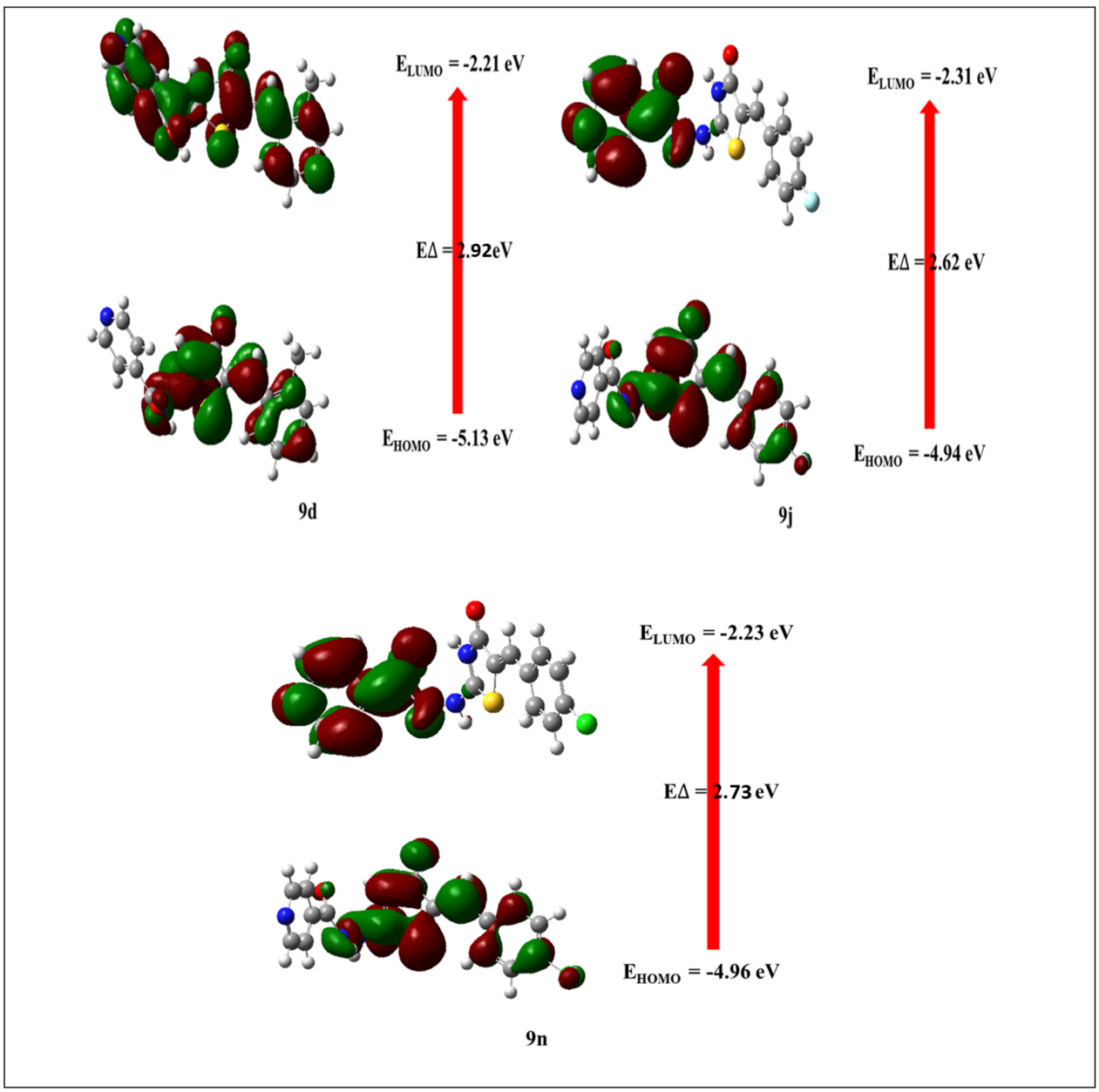

Fig. 8 Illustration of the FMOs of compounds **9d**, **9j**, and **9n**.

© 2025 The Author(s). Published by the Royal Society of Chemistry

Open Access Article. Published on 01 September 2025. Downloaded on 2/11/2026 10:32:12 PM. This article is licensed under a Creative Commons Attribution-NonCommercial 3.0 Unported Licence.

INH–Rh hybrids displayed promising *in vitro* antitubercular activity, none surpassed the potency of parent isoniazid (MIC = 0.039 μg ml^{-1}). Notably, compound **9d** exhibited low cytotoxicity against THP-1 macrophages, resulting in a favorable selectivity index. The loss of activity of these compounds against KatG-mutant strains and their reduced efficacy in InhA-overexpressing *Mtb* strains strongly suggest that their mechanism of action involves InhA inhibition, similar to that of INH. However, the KatG-dependency of the hybrids somehow diminishes their interest, as they are unlikely to overcome resistance in INH-resistant clinical strains carrying mutations in KatG. In addition, DFT calculations provided valuable insights into frontier molecular orbitals and global reactivity parameters, aiding the interpretation of electronic properties related to biological activity. Collectively, these findings underscore the potential of INH–Rh hybrids, particularly compound **9d**, as promising leads for the development of new anti-TB agents. Further structural optimization could lead to the identification of potent lead compounds with improved therapeutic profiles.

4. Materials and methods

4.1. Chemicals and reagents

The intermediates and INH–Rh molecular hybrids were synthesized using chemicals purchased from Merck, CRD, Sigma, and Aldrich without purification. To monitor the progress of the reaction a Thin Layer Chromatography (TLC 60 F_{254}) silica gel plates were used. The ^{1}H and ^{13}C NMR spectroscopy were used to characterize precursor **8a–t**. The final products were elucidated using various spectroscopic techniques, *viz.*, IR, ^{1}H, ^{13}C NMR, and HRMS. 2D NMR experiment heteronuclear single quantum coherence spectroscopy (HSQC) and heteronuclear multiple bond correlation (HMBC) were performed for compound **8b**. The NMRs were recorded on a Bruker Avance-III spectrometer (600 and 150 MHz). In addition to chemical shifts in ppm, coupling constants (*J*) in Hz are also reported. The multiplicities are reported as follows: singlet (s), doublet (d), doublet of doublets (dd), quartet (q), multiplet (m), triplet (t), and broad singlet (brs). High-resolution mass spectra (HRMS) were recorded on a micro-mass ESI TOF (time of flight) mass spectrometer. The digital melting point apparatus was used to record the melting point. Using the ATR technique, the Fourier transform infrared (FTIR) spectra were recorded in the spectral range of 400–4000 cm^{-1} on PerkinElmer (FTIR spectrum II).

4.2. General procedures for the synthesis of 3a–t

The intermediates I (**3a–t**) were prepared according to the reported document.[67] In a round-bottom flask, a mixture of aldehyde **1a–t** (1.0 eq.), rhodanine **2** (1.0 eq.), and sodium acetate (1 eq.) was stirred in the presence of acetic acid for 7 h under reflux at 120 °C. Following the end of the reaction, the resultant solution was allowed to cool, and the precipitates were filtered out using a Buchner funnel. The product was purified in ethanol by filtering out and recrystallizing the solid.

4.3. General procedures for the synthesis of 8a–t

A mixture of benzylidene **3a–t** (1.0 eq.) and trimethylamine (1.5 eq.) was stirred in DCM at room temperature for 10 min, before adding methyl iodide (1.5 eq.) dropwise. Further, the mixture was stirred for 2 h. After completion of the reaction (confirmed by TLC), the solvent was evaporated using a rotor evaporator. The solid product was quenched with water and filtered out using a Buchner funnel. The compounds were purified by recrystallization using ethanol.

4.4. General procedures for the synthesis of INH–Rh molecular hybrids 9a–t

In a round-bottom flask of 50 ml, intermediate **8a–t** (1.0 eq.) and INH (1.0 eq.) were stirred at room temperature for 24 h. The reaction was analyzed by TLC. After the completion of the reaction, 10 ml of ethanol was added to the reaction mixture. The solid formed was filtered using the Buchner funnel and purified further by recrystallization using ethanol.

4.5. Analytical data

Provided in the SI.

4.6. Biological assays

4.6.1. Culture conditions. The pantothenate-auxotrophic *Mtb* $mc^{2}6230$ strain and KatG mutants[95] were grown in Middlebrook 7H9 broth supplemented with 10% OADC, 0.025% tyloxapol and 109 μM pantothenic (complete 7H9) at 37 °C without agitation.[96] The $mc^{2}6230$ strain carrying the pMV261_*inhA*[97] or containing the empty plasmid pMV261 was grown using the same medium supplemented with 50 μg per ml kanamycin.

4.6.2. Drug susceptibility testing. The MIC was defined as the lowest concentration of compound inhibiting 99% of bacterial growth, at which no change in turbidity was observed, and was performed in 7H9 broth supplemented with 10% OADC, 0.025% tyloxapol, and 109 μM pantothenic acid at 37 °C without agitation. For MIC determination, a log-phase culture was diluted to an $OD_{600} = 0.05$ in complete 7H9 and deposited in 96-well plates. Compounds were then directly added (2 μl per well of a 20 mg ml^{-1} or 10 mg per ml stock solution) to the first-row wells containing 198 μl of bacteria. Serial 2-fold dilutions were then completed, starting from the first row. Plates were wrapped in parafilm and then placed in a 37 °C incubator and observed after 6 days of incubation. Control wells included DMSO as vehicle control, in which bacterial growth was not inhibited (as for untreated wells). INH was included as a reference drug. Experiments were conducted three times in duplicate.

4.6.3. Cytotoxicity assay. Human THP-1 monocytes, obtained from ATCC: ATCC® TIB-202™, were grown in RPMI medium supplemented with 10% Fetal Bovine Serum (Sigma-Aldrich) and incubated at 37 °C with 5% CO_2. Cells were differentiated with 20 ng per ml phorbol myristate acetate in a 96-well plate (2×10^{4} cells per well) for 48 h and exposed to decreasing concentrations (ranging from 100 μg ml^{-1} to 0.78 μg

Open Access Article. Published on 01 September 2025. Downloaded on 2/11/2026 10:32:12 PM. This article is licensed under a Creative Commons Attribution-NonCommercial 3.0 Unported Licence.

ml^{-1}) of the tested compounds. Following incubation (24 or 72 h), 10% v/v resazurin was added to each well and left to incubate for a few hours at 37 °C with 5% CO_2. Data were measured using a fluorescent plate reader (excitation 540 nm, emission 590 nm). Results are the mean of two independent experiments done in duplicate.

4.7. Computational studies

4.7.1. Molecular docking. Molecular docking was conducted using the Schrödinger suite (2022-1 release) with calculations based on the OPLS4 forcefield. Firstly, the structure of Mtb enoyl-acyl carrier protein reductase (InhA; PDB ID: 4QXM) was obtained from the Protein Data Bank and corrected by adding missing hydrogens, side chains, and loops using Prime.[98] Epik[99] was used to generate tautomers and heteroatomic states at pH 7.0 ± 2.0, and deleting water molecules that are 5 Å away from the binding cavity. The hydrogen network was then optimized and minimized to an RMSD of 0.3 Å. Subsequently, the binding site was minimized using Prime. Compounds for docking were drawn, saved as ChemDraw files, imported into the workspace, and prepared using the LigPrep module to generate 3D models with the lowest energy conformation. The Induced Fit Protocol (IFD) module was employed to dock these compounds into the active site of InhA. This process involved defining the ligand box by selecting a box using the centroid of selected residues with dimensions under 20 Å, and performing conformational sampling within a 2.5 kcal mol^{-1} energy range. Ligands were docked with Glide, and poses were refined by adjusting side chain conformations using Prime. Poses with energies up to 30 kcal mol^{-1} were redocked, and the top 10 poses were selected for evaluation. The best pose for each protein–ligand complex was chosen based on docking scores, IFD scores, Glide e-model, and Glide energy.

4.7.2. ADME/T. The SwissADME web tools **https://www.swissadme.ch/**and QikPro were utilized in this study to assess the absorption, distribution, metabolism, and excretion characteristics of the drug candidates. Additionally, the pkCSM online portal **https://biosig.lab.uq.edu.au/pkcsm/**was used for ADMET studies. This data is crucial to the drug approval process as it provides insights into the drug-likeness of the compounds tested. The default predictors provided by the tool were used for analysis.

4.7.3. DFT studies. To optimize the energy of molecules **9d**, **9j**, **9n**, and INH, the Gaussian 16W[100] software was used. To identify the optimal structural parameters, the B3LYP functional along with the 6-31G++ (d, p) basis set was employed. Gauss View 6.0 software was used to analyze the output files.

Conflicts of interest

There are no conflicts to declare.

Data availability

Supplementary information: The authors declare that all the data generated in this work has either been provided in the manuscript or the SI data file. Also, all the information used from the literature has been appropriately cited. See DOI: **https://doi.org/10.1039/d5ra03641k**.

Acknowledgements

PS gratefully acknowledges the National Research Foundation (SA) for a Competitive Grant for rated researchers (Grant Number: SRUG2204092857). GK is thankful to NRF-SA for the doctoral research grant (PMDS230505102841). All authors are grateful to the Centre for High-Performance Computing (CHPC), Cape Town, for the computational resources used in this work. The authors wish to thank the support of the Fondation pour la Recherche Médicale (Equipe FRM EQU202103012588) to LK and Claire Hamela for the help in statistical analyses.

References

1 M. A. Martinez-Grau, I. C. G. Valcarcel, J. V. Early, R. K. Gessner, C. S. de Melo, E. M. M. de la Nava, A. Korkegian, Y. Ovechkina, L. Flint and A. Gravelle, Synthesis and biological evaluation of aryl-oxadiazoles as inhibitors of Mycobacterium tuberculosis, *Bioorg. Med. Chem. Lett.*, 2018, **28**(10), 1758–1764.

2 V. U. Jeankumar, J. Renuka, P. Santosh, V. Soni, J. P. Sridevi, P. Suryadevara, P. Yogeeswari and D. Sriram, Thiazole–aminopiperidine hybrid analogues: Design and synthesis of novel Mycobacterium tuberculosis GyrB inhibitors, *Eur. J. Med. Chem.*, 2013, **70**, 143–153.

3 M. Sabbah, V. Mendes, R. G. Vistal, D. M. Dias, M. Záhorszká, K. Mikusova, J. Korduláková, A. G. Coyne, T. L. Blundell and C. Abell, Fragment-based design of Mycobacterium tuberculosis InhA inhibitors, *J. Med. Chem.*, 2020, **63**(9), 4749–4761.

4 V. Singh, G. A. Dziwornu and K. Chibale, The implication of Mycobacterium tuberculosis-mediated metabolism of targeted xenobiotics, *Nat. Rev. Chem.*, 2023, **7**(5), 340–354.

5 S. Bagcchi, WHO's global tuberculosis report 2022, *Lancet Microbe*, 2023, **4**(1), e20.

6 Y.-L. Fan, X.-H. Jin, Z.-P. Huang, H.-F. Yu, Z.-G. Zeng, T. Gao and L.-S. Feng, Recent advances of imidazole-containing derivatives as anti-tubercular agents, *Eur. J. Med. Chem.*, 2018, **150**, 347–365.

7 L. Cilloni, H. Fu, J. Vesga, D. Dowdy, C. Pretorius, S. Ahmedov, S. Nair, A. Mosneaga, E. Masini and S. Sahu, The Potential Impact of the COVID-19 Pandemic on the Tuberculosis Epidemic: A Modelling Analysis, *EClinicalMedicine*, 2020, 100603–100611.

8 S. H. Siddiqui, A. Sarfraz, A. Rizvi, F. Shaheen, M. T. Yousafzai and S. A. Ali, Global variation of COVID-19 mortality rates in the initial phase, *Osong Public Health Res. Perspect.*, 2021, **12**(2), 64.

9 Y. Zhang, L. Zhang, W. Gao, M. Li, Q. Luo, Y. Xiang and K. Bao, The impact of COVID-19 pandemic on reported tuberculosis incidence and mortality in China: An

© 2025 The Author(s). Published by the Royal Society of Chemistry

Open Access Article. Published on 01 September 2025. Downloaded on 2/11/2026 10:32:12 PM. This article is licensed under a Creative Commons Attribution-NonCommercial 3.0 Unported Licence.

interrupted time series analysis, *J. Glob. Health*, 2023, **13**, 06043–06051.

10 E. Pontali, M. C. Raviglione and G. B. Migliori, Regimens to treat multidrug-resistant tuberculosis: past, present and future perspectives, *Eur. Respir. Rev.*, 2019, **28**, 190035–190040.

11 B. Kushwaha, N. D. Kushwaha, T. Parish, J. Guzman, A. Kajee, M. S. Shaikh, I. Kehinde, V. A. Obakachi, T. K. Pathan and S. R. Shinde, A New Class of Linezolid-Based Molecules as Potential Antimicrobial and Antitubercular Agents: A Rational Approach, *ChemistrySelect*, 2021, **6**(13), 3065–3074.

12 R. Bairwa, M. Kakwani, N. R. Tawari, J. Lalchandani, M. Ray, M. Rajan and M. S. Degani, Novel molecular hybrids of cinnamic acids and guanylhydrazones as potential antitubercular agents, *Bioorg. Med. Chem. Lett.*, 2010, **20**(5), 1623–1625.

13 C. Soares de Melo, V. Singh, A. Myrick, S. B. Simelane, D. Taylor, C. Brunschwig, N. Lawrence, D. Schnappinger, C. A. Engelhart and A. Kumar, Antitubercular 2-Pyrazolylpyrimidinones: Structure–Activity Relationship and Mode-of-Action Studies, *J. Med. Chem.*, 2021, **64**(1), 719–740.

14 I. Abubakar, M. Zignol, D. Falzon, M. Raviglione, L. Ditiu, S. Masham, I. Adetifa, N. Ford, H. Cox and S. D. Lawn, Drug-resistant tuberculosis: time for visionary political leadership, *Lancet Infect. Dis.*, 2013, **13**(6), 529–539.

15 H. Zhao, Y. Lu, L. Sheng, Z. Yuan, B. Wang, W. Wang, Y. Li, C. Ma, X. Wang and D. Zhang, Discovery of fluorine-containing benzoxazinyl-oxazolidinones for the treatment of multidrug resistant tuberculosis, *ACS Med. Chem. Lett.*, 2017, **8**(5), 533–537.

16 D. Murugesan, P. C. Ray, T. Bayliss, G. A. Prosser, J. R. Harrison, K. Green, C. Soares de Melo, T.-S. Feng, L. J. Street and K. Chibale, 2-Mercapto-Quinazolinones as inhibitors of type II NADH dehydrogenase and Mycobacterium tuberculosis: structure–activity relationships, mechanism of action and absorption, distribution, metabolism, and excretion characterization, *ACS Infect. Dis.*, 2018, **4**(6), 954–969.

17 L. P. Khonde, R. Müller, G. A. Boyle, V. Reddy, A. T. Nchinda, C. J. Eyermann, S. Fienberg, V. Singh, A. Myrick and E. Abay, 1, 3-Diarylpyrazolyl-acylsulfonamides as potent anti-tuberculosis agents targeting cell wall biosynthesis in Mycobacterium tuberculosis, *J. Med. Chem.*, 2021, **64**(17), 12790–12807.

18 L. J. Alderwick, J. Harrison, G. S. Lloyd and H. L. Birch, The mycobacterial cell wall—peptidoglycan and arabinogalactan, *Cold Spring Harb. Perspect. Med.*, 2015, **5**(8), a021113.

19 K. A. Abrahams and G. S. Besra, Synthesis and recycling of the mycobacterial cell envelope, *Curr. Opin. Microbiol.*, 2021, **60**, 58–65.

20 C. Vilchèze, F. Wang, M. Arai, M. H. Hazbón, R. Colangeli, L. Kremer, T. R. Weisbrod, D. Alland, J. C. Sacchettini and W. R. Jacobs Jr, Transfer of a point mutation in Mycobacterium tuberculosis inhA resolves the target of isoniazid, *Nat. Med.*, 2006, **12**(9), 1027–1029.

21 C. Vilchèze, Mycobacterial cell wall: a source of successful targets for old and new drugs, *Appl. Sci.*, 2020, **10**(7), 2278.

22 A. N. Unissa, S. Subbian, L. E. Hanna and N. Selvakumar, Overview on mechanisms of isoniazid action and resistance in Mycobacterium tuberculosis, *Infect. Genet. Evol.*, 2016, **45**, 474–492.

23 C. Zhu, Y. Liu, L. Hu, M. Yang and Z.-G. He, Molecular mechanism of the synergistic activity of ethambutol and isoniazid against Mycobacterium tuberculosis, *J. Biol. Chem.*, 2018, **293**(43), 16741–16750.

24 A. M. Ginsberg and M. Spigelman, Challenges in tuberculosis drug research and development, *Nat. Med.*, 2007, **13**(3), 290–294.

25 L. J. Yin, A. K. D. bin Ahmad Kamar, G. T. Fung, C. T. Liang and V. R. Avupati, Review of anticancer potentials and structure-activity relationships (SAR) of rhodanine derivatives, *Biomed. Pharmacother.*, 2022, **145**, 112406.

26 N. A. Abdel Hafez, M. A. Elsayed, M. M. El-Shahawi, G. E. Awad and K. A. Ali, Synthesis and antimicrobial activity of new thiazolidine-based heterocycles as rhodanine analogues, *J. Heterocycl. Chem.*, 2018, **55**(3), 685–691.

27 A. Chaurasyia, P. Chawla, V. Monga and G. Singh, Rhodanine derivatives: An insight into the synthetic and medicinal perspectives as antimicrobial and antiviral agents, *Chem. Biol. Drug Des.*, 2023, **101**(3), 500–549.

28 G. Kumar, P. Parasuraman, S. K. Sharma, T. Banerjee, K. Karmodiya, N. Surolia and A. Surolia, Discovery of a rhodanine class of compounds as inhibitors of Plasmodium falciparum enoyl-acyl carrier protein reductase, *J. Med. Chem.*, 2007, **50**(11), 2665–2675.

29 A. K. D. bin Ahmad Kamar, L. J. Yin, C. T. Liang, G. T. Fung and V. R. Avupati, Rhodanine scaffold: A review of antidiabetic potential and structure–activity relationships (SAR), *Med. Drug Discovery*, 2022, **15**, 100131.

30 D. D. Subhedar, M. H. Shaikh, B. B. Shingate, L. Nawale, D. Sarkar, V. M. Khedkar, F. A. K. Khan and J. N. Sangshetti, Graphical Abstract Quinolidene-Rhodanine Conjugates: Facile Synthesis and Biological Evaluation, *Eur. J. Med. Chem.*, 2017, **125**, 385–399.

31 S. Cheng, Y. Zou, X. Chen, J. Chen, B. Wang, J. Tian, F. Ye, Y. Lu, H. Huang and Y. Lu, Design, synthesis and biological evaluation of 3-substituted-2-thioxothiazolidin-4-one (rhodanine) derivatives as antitubercular agents against Mycobacterium tuberculosis protein tyrosine phosphatase B, *Eur. J. Med. Chem.*, 2023, **258**, 115571.

32 S. G. Alegaon, K. R. Alagawadi, P. V. Sonkusare, S. M. Chaudhary, D. H. Dadwe and A. S. Shah, Novel imidazo [2,1-*b*][1,3,4] thiadiazole carrying rhodanine-3-acetic acid as potential antitubercular agents, *Bioorg. Med. Chem. Lett.*, 2012, **22**(5), 1917–1921.

33 M. S. Shaikh, A. M. Kanhed, B. Chandrasekaran, M. B. Palkar, N. Agrawal, C. Lherbet, G. A. Hampannavar and R. Karpoormath, Discovery of novel N-methyl carbazole tethered rhodanine derivatives as direct

Open Access Article. Published on 01 September 2025. Downloaded on 2/11/2026 10:32:12 PM. This article is licensed under a Creative Commons Attribution-NonCommercial 3.0 Unported Licence.

inhibitors of Mycobacterium tuberculosis InhA, *Bioorg. Med. Chem. Lett.*, 2019, **29**(16), 2338–2344.
34 L. Slepikas, G. Chiriano, R. Perozzo, S. Tardy, A. Kranjc, O. Patthey-Vuadens, H. Ouertatani-Sakouhi, S. Kicka, C. F. Harrison and T. Scrignari, In silico driven design and synthesis of rhodanine derivatives as novel antibacterials targeting the enoyl reductase InhA, *J. Med. Chem.*, 2016, **59**(24), 10917–10928.
35 K. Chauhan, M. Sharma, J. Saxena, S. V. Singh, P. Trivedi, K. Srivastava, S. K. Puri, J. Saxena, V. Chaturvedi and P. M. Chauhan, Synthesis and biological evaluation of a new class of 4-aminoquinoline–rhodanine hybrid as potent anti-infective agents, *Eur. J. Med. Chem.*, 2013, **62**, 693–704.
36 N. Trotsko, Antitubercular properties of thiazolidin-4-ones–A review, *Eur. J. Med. Chem.*, 2021, **215**, 113266.
37 K. Chauhan, M. Sharma, P. Trivedi, V. Chaturvedi and P. M. Chauhan, New class of methyl tetrazole based hybrid of (Z)-5-benzylidene-2-(piperazin-1-yl) thiazol-4 (% H)-one as potent antitubercular agents, *Bioorg. Med. Chem. Lett.*, 2014, **24**(17), 4166–4170.
38 V. Šlachtová, M. Šebela, E. Torfs, L. Oorts, D. Cappoen, K. Berka, V. Bazgier and L. Brulikova, Novel thiazolidinedione-hydroxamates as inhibitors of Mycobacterium tuberculosis virulence factor Zmp1, *Eur. J. Med. Chem.*, 2020, **185**, 111812.
39 M. Mori, D. Deodato, M. Kasula, D. M. Ferraris, A. Sanna, A. De Logu, M. Rizzi and M. Botta, Design, synthesis, SAR and biological investigation of 3-(carboxymethyl) rhodanine and aminothiazole inhibitors of Mycobacterium tuberculosis Zmp1, *Bioorg. Med. Chem. Lett.*, 2018, **28**(4), 637–641.
40 D. D. Subhedar, M. H. Shaikh, B. B. Shingate, L. Nawale, D. Sarkar, V. M. Khedkar, F. A. K. Khan and J. N. Sangshetti, Quinolidene-rhodanine conjugates: Facile synthesis and biological evaluation, *Eur. J. Med. Chem.*, 2017, **125**, 385–399.
41 M. Naufal, E. Hermawati, Y. M. Syah, A. T. Hidayat, I. W. Hidayat and J. Al-Anshori, Structure–Activity Relationship Study and Design Strategies of Hydantoin, Thiazolidinedione, and Rhodanine-Based Kinase Inhibitors: A Two-Decade Review, *ACS Omega*, 2024, **9**, 4186–4209.
42 M. Azizmohammadi, M. Khoobi, A. Ramazani, S. Emami, A. Zarrin, O. Firuzi, R. Miri and A. Shafiee, 2H-chromene derivatives bearing thiazolidine-2, 4-dione, rhodanine or hydantoin moieties as potential anticancer agents, *Eur. J. Med. Chem.*, 2013, **59**, 15–22.
43 G.-C. Wang, Y.-P. Peng, Z.-Z. Xie, J. Wang and M. Chen, Synthesis, α-glucosidase inhibition and molecular docking studies of novel thiazolidine-2, 4-dione or rhodanine derivatives, *MedChemComm*, 2017, **8**(7), 1477–1484.
44 T. Tomasic and L. P. Masic, Rhodanine as a privileged scaffold in drug discovery, *Curr. Med. Chem.*, 2009, **16**(13), 1596–1629.
45 N. Khan, G. Gautam and A. K. Gupta, Synthesis and biological evaluation of some new rhodanine analogues as aldose reductase inhibitors (ARIs), *J. Drug Deliv. Therapeut.*, 2019, **9**(1-s), 161–167.
46 S. M. Mousavi, M. Zarei, S. A. Hashemi, A. Babapoor and A. M. Amani, A conceptual review of rhodanine: current applications of antiviral drugs, anticancer and antimicrobial activities, *Artif. Cell Nanomed. Biotechnol.*, 2019, **47**(1), 1132–1148.
47 R. S. Bhatti, S. Shah, P. Krishan and J. S. Sandhu, Recent pharmacological developments on rhodanines and 2, 4-thiazolidinediones, *Int. J. Med. Chem. Anal.*, 2013, **2013**, 793260–793275.
48 S. Sreelatha, U. Nagarajan and S. Natarajan, Protein targets in Mycobacterium tuberculosis and their inhibitors for therapeutic implications: A narrative review, *Int. J. Biol. Macromol.*, 2023, 125022.
49 Y. Teneva, R. Simeonova, V. Valcheva and V. T. Angelova, Recent advances in anti-tuberculosis drug discovery based on hydrazide–hydrazone and thiadiazole derivatives targeting inhA, *Pharmaceuticals*, 2023, **16**(4), 484.
50 C. Vilchèze and W. R. Jacobs Jr, The isoniazid paradigm of killing, resistance, and persistence in Mycobacterium tuberculosis, *J. Mol. Biol.*, 2019, **431**(18), 3450–3461.
51 P. Purkan, I. Ihsanawati, D. Natalia, Y. Syah, D. Retnoningrum and I. Siswanto, Molecular analysis of katG encoding catalase-peroxidase from clinical isolate of isoniazid-resistant Mycobacterium tuberculosis, *J. Med. Life.*, 2018, **11**(2), 160.
52 T. H. Reingewertz, T. Meyer, F. McIntosh, J. Sullivan, M. Meir, Y.-F. Chang, M. A. Behr and D. Barkan, Differential sensitivity of mycobacteria to isoniazid is related to differences in KatG-mediated enzymatic activation of the drug, *Antimicrob. Agents Chemother.*, 2020, **64**(2), e01899.
53 M. Martínez-Hoyos, E. Perez-Herran, G. Gulten, L. Encinas, D. Álvarez-Gómez, E. Alvarez, S. Ferrer-Bazaga, A. García-Pérez, F. Ortega and I. Angulo-Barturen, Antitubercular drugs for an old target: GSK693 as a promising InhA direct inhibitor, *EBioMedicine*, 2016, **8**, 291–301.
54 C. Viegas-Junior, A. Danuello, V. da Silva Bolzani, E. J. Barreiro and C. A. M. Fraga, Molecular hybridization: a useful tool in the design of new drug prototypes, *Curr. Med. Chem.*, 2007, **14**(17), 1829–1852.
55 V. S. Gontijo, F. P. D. Viegas, C. J. Ortiz, M. de Freitas Silva, C. M. Damasio, M. C. Rosa, T. G. Campos, D. S. Couto, K. S. Tranches Dias and C. Viegas, Molecular hybridization as a tool in the design of multi-target directed drug candidates for neurodegenerative diseases, *Curr. Neuropharmacol.*, 2020, **18**(5), 348–407.
56 L. L. Fershtat and N. N. Makhova, Molecular hybridization tools in the development of furoxan-based NO-donor prodrugs, *ChemMedChem*, 2017, **12**(9), 622–638.
57 O. Ebenezer, A. Singh-Pillay, N. A. Koorbanally and P. Singh, Antibacterial evaluation and molecular docking studies of pyrazole–thiosemicarbazones and their pyrazole–

 © 2025 The Author(s). Published by the Royal Society of Chemistry

Open Access Article. Published on 01 September 2025. Downloaded on 2/11/2026 10:32:12 PM. This article is licensed under a Creative Commons Attribution-NonCommercial 3.0 Unported Licence.

thiazolidinone conjugates, *Mol. Diversity*, 2021, **25**, 191–204.

58 P. Singh, B. Jaiyeola, N. Kerru, O. Ebenezer and A. Bissessur, A review of recent advancements in anti-tubercular molecular hybrids, *Curr. Med. Chem.*, 2017, **24**(37), 4180–4212.

59 R. Raj, P. Singh, P. Singh, J. Gut, P. J. Rosenthal and V. Kumar, Azide-alkyne cycloaddition en route to 1H-1, 2, 3-triazole-tethered 7-chloroquinoline-isatin chimeras: Synthesis and antimalarial evaluation, *Eur. J. Med. Chem.*, 2013, **62**, 590–596.

60 B. Yu, P.-P. Qi, X.-J. Shi, R. Huang, H. Guo, Y.-C. Zheng, D.-Q. Yu and H.-M. Liu, Efficient synthesis of new antiproliferative steroidal hybrids using the molecular hybridization approach, *Eur. J. Med. Chem.*, 2016, **117**, 241–255.

61 N. Kerru, P. Singh, N. Koorbanally, R. Raj and V. Kumar, Recent advances (2015–2016) in anticancer hybrids, *Eur. J. Med. Chem.*, 2017, **142**, 179–212.

62 P. Awolade, N. Cele, N. Kerru and P. Singh, Synthesis, antimicrobial evaluation, and in silico studies of quinoline—1 H-1, 2, 3-triazole molecular hybrids, *Mol. Divers.*, 2021, **25**, 2201–2218.

63 K. D. Patel, R. H. Vekariya, N. P. Prajapati, D. B. Patel, H. D. Patel, T. Shaikh, D. P. Rajani, S. Rajani, N. S. Shah and D. Jhala, Synthesis of N'-(Quinazolin-4-yl) isonicotinohydrazides and their biological screening, docking and ADME studies, *Arab. J. Chem.*, 2020, **13**(1), 1986–2000.

64 E. K. Aslan, V. S. Krishna, S. J. Armaković, S. Armaković, O. Şahin, T. Tønjum and M. G. Gündüz, Linking azoles to isoniazid via hydrazone bridge: Synthesis, crystal structure determination, antitubercular evaluation and computational studies, *J. Mol. Liq.*, 2022, **354**, 118873.

65 Z. M. Elsayed, W. M. Eldehna, M. M. Abdel-Aziz, M. A. El Hassab, E. B. Elkaeed, T. Al-Warhi, H. A. Abdel-Aziz, S. M. Abou-Seri and E. R. Mohammed, Development of novel isatin–nicotinohydrazide hybrids with potent activity against susceptible/resistant Mycobacterium tuberculosis and bronchitis causing–bacteria, *J. Enzym. Inhib. Med. Chem.*, 2021, **36**(1), 384–392.

66 G. Kumar, P. Seboletswe, S. Mishra, N. Manhas, S. Ghumran, N. Kerru, F. Roquet-Banères, M. Foubert, L. Kremer and G. Bhargava, Isoniazid-Dihydropyrimidinone Molecular Hybrids: Design, Synthesis, Antitubercular Activity, and Cytotoxicity Investigations with Computational Validation, *ChemMedChem*, 2025, **20**(11), e202400949.

67 M. G. Salem, Y. M. A. Aziz, M. Elewa, M. S. Nafie, H. A. Elshihawy and M. M. Said, Synthesis, molecular modeling, selective aldose reductase inhibition and hypoglycemic activity of novel meglitinides, *Bioorg. Chem.*, 2021, **111**, 104909.

68 D. A. Rozwarski, G. A. Grant, D. H. Barton, W. R. Jacobs Jr and J. C. Sacchettini, Modification of the NADH of the isoniazid target (InhA) from Mycobacterium tuberculosis, *Science*, 1998, **279**(5347), 98–102.

69 A. Guardia, G. Gulten, R. Fernandez, J. Gómez, F. Wang, M. Convery, D. Blanco, M. Martínez, E. Pérez-Herrán and M. Alonso, N-Benzyl-4-((heteroaryl) methyl) benzamides: A new class of direct NADH-dependent 2-trans enoyl–acyl carrier protein reductase (InhA) inhibitors with antitubercular activity, *ChemMedChem*, 2016, **11**(7), 687–701.

70 N. Phusi, R. Sato, T. Ezawa, S. Tomioka, C. Hanwarinroj, B. Khamsri, P. Kamsri, A. Punkvang, P. Pungpo and N. Kurita, Specific interactions between 2-trans enoyl-acyl carrier protein reductase and its ligand: Protein-ligand docking and ab initio fragment molecular orbital calculations, *J. Mol. Graph. Model.*, 2019, **88**, 299–308.

71 M. Er-Rajy, M. El Fadili, S. Mujwar, S. Zarougui and M. Elhallaoui, Design of novel anti-cancer drugs targeting TRKs inhibitors based 3D QSAR, molecular docking and molecular dynamics simulation, *J. Biomol. Struct. Dyn.*, 2023, **41**(21), 11657–11670.

72 D. F. Veber, S. R. Johnson, H.-Y. Cheng, B. R. Smith, K. W. Ward and K. D. Kopple, Molecular properties that influence the oral bioavailability of drug candidates, *J. Med. Chem.*, 2002, **45**(12), 2615–2623.

73 M. Athalye, D. Teli, A. Sharma and M. Patel, Anti-Epileptic Drug-Lipid Conjugates for Delivery to the Brain: In Silico ADMET Prediction, Molecular Docking and Molecular Dynamics Simulations, *ChemistrySelect*, 2023, **8**(34), e202301701.

74 H. Hadni, M. Bakhouch and M. Elhallaoui, 3D-QSAR, molecular docking, DFT and ADMET studies on quinazoline derivatives to explore novel DHFR inhibitors, *J. Biomol. Struct. Dyn.*, 2023, **41**(1), 161–175.

75 M. A. H. Hosseini, A. A. Alizadeh and A. Shayanfar, Prediction of the First-Pass Metabolism of a Drug After Oral Intake Based on Structural Parameters and Physicochemical Properties, *Eur. J. Drug Metab. Pharmacokinet.*, 2024, 1–17.

76 O. Daoui, H. Nour, O. Abchir, S. Elkhattabi, M. Bakhouch and S. Chtita, A computer-aided drug design approach to explore novel type II inhibitors of c-Met receptor tyrosine kinase for cancer therapy: QSAR, molecular docking, ADMET and molecular dynamics simulations, *J. Biomol. Struct. Dyn.*, 2023, **41**(16), 7768–7785.

77 Y. Han, J. Zhang, C. Q. Hu, X. Zhang, B. Ma and P. Zhang, In silico ADME and toxicity prediction of ceftazidime and its impurities, *Front. Pharmacol.*, 2019, **10**, 434.

78 P. O. Lohohola, B. M. Mbala, S.-M. N. Bambi, D. T. Mawete, A. Matondo and J. G. M. Mvondo, In silico ADME/T properties of quinine derivatives using SwissADME and pkCSM webservers, *Int. J. Trop. Dis. Health*, 2021, **42**(11), 1–12.

79 D. Osmaniye, I. Ahmad, B. N. Sağlık, S. Levent, H. M. Patel, Y. Ozkay and Z. A. Kaplancıklı, Design, synthesis and molecular docking and ADME studies of novel hydrazone derivatives for AChE inhibitory, BBB permeability and antioxidant effects, *J. Biomol. Struct. Dyn.*, 2023, **41**(18), 9022–9038.

Open Access Article. Published on 01 September 2025. Downloaded on 2/11/2026 10:32:12 PM. This article is licensed under a Creative Commons Attribution-NonCommercial 3.0 Unported Licence.

80 F. A. Resende, W. Vilegas, L. C. Dos Santos and E. A. Varanda, Mutagenicity of flavonoids assayed by bacterial reverse mutation (Ames) test, *Molecules*, 2012, **17**(5), 5255–5268.
81 C.-G. Zhan, J. A. Nichols and D. A. Dixon, Ionization potential, electron affinity, electronegativity, hardness, and electron excitation energy: molecular properties from density functional theory orbital energies, *J. Phys. Chem. A*, 2003, **107**(20), 4184–4195.
82 F. De Proft, W. Langenaeker and P. Geerlings, Ab initio determination of substituent constants in a density functional theory formalism: calculation of intrinsic group electronegativity, hardness, and softness, *J. Phys. Chem.*, 1993, **97**(9), 1826–1831.
83 J. Khan, S. A. Sakib, S. Mahmud, Z. Khan, M. N. Islam, M. A. Sakib, T. B. Emran and J. Simal-Gandara, Identification of potential phytochemicals from Citrus limon against main protease of SARS-CoV-2: Molecular docking, molecular dynamic simulations and quantum computations, *J. Biomol. Struct. Dyn.*, 2022, **40**(21), 10741–10752.
84 S. Gunasekaran, R. A. Balaji, S. Kumeresan, G. Anand and S. Srinivasan, Experimental and theoretical investigations of spectroscopic properties of N-acetyl-5-methoxytryptamine, *Can. J. Anal. Sci. Spectrosc.*, 2008, **53**(4), 149–162.
85 V. Choudhary, A. Bhatt, D. Dash and N. Sharma, DFT calculations on molecular structures, HOMO–LUMO study, reactivity descriptors and spectral analyses of newly synthesized diorganotin (IV) 2-chloridophenylacetohydroxamate complexes, *J. Comput. Chem.*, 2019, **40**(27), 2354–2363.
86 V. J. Reeda and V. B. Jothy, Vibrational spectroscopic, quantum computational (DFT), reactivity (ELF, LOL and Fukui), molecular docking studies and molecular dynamic simulation on (6-methoxy-2-oxo-2H-chromen-4-yl) methyl morpholine-4-carbodithioate, *J. Mol. Liq.*, 2023, **371**, 121147.
87 N. Kerru, L. Gummidi, S. V. Bhaskaruni, S. N. Maddila, P. Singh and S. B. Jonnalagadda, A comparison between observed and DFT calculations on structure of 5-(4-chlorophenyl)-2-amino-1, 3, 4-thiadiazole, *Sci. Rep.*, 2019, **9**(1), 19280.
88 A. Rani, S. Kumar, J. Legac, A. A. Adeniyi, P. Awolade, P. Singh, P. J. Rosenthal and V. Kumar, Design, synthesis, heme binding and density functional theory studies of isoindoline-dione-4-aminoquinolines as potential antiplasmodials, *Future Med. Chem.*, 2020, **12**(3), 193–205.
89 J.-i. Aihara, Reduced HOMO−LUMO gap as an index of kinetic stability for polycyclic aromatic hydrocarbons, *J. Phys. Chem. A*, 1999, **103**(37), 7487–7495.
90 D. Chun, Y. Cheng and F. Wudl, The most stable and fully characterized functionalized heptacene, *Angew. Chem.*, 2008, **120**(44), 8508–8513.
91 O. E. Oyeneyin, A. Ibrahim, N. Ipinloju, A. J. Ademoyegun and N. D. Ojo, Insight into the corrosion inhibiting potential and anticancer activity of 1-(4-methoxyphenyl)-5-methyl-N′-(2-oxoindolin-3-ylidene)-1H-1, 2, 3-triazole-4-carbohydrazide via computational approaches, *J. Biomol. Struct. Dyn.*, 2023, 1–18.
92 S. Deswal, R. K. Tittal, D. G. Vikas, K. Lal and A. Kumar, 5-Fluoro-1H-indole-2, 3-dione-triazoles-synthesis, biological activity, molecular docking, and DFT study, *J. Mol. Struct.*, 2020, **1209**, 127982.
93 R. Galeazzi, C. Marucchini, M. Orena and C. Zadra, Stereoelectronic properties and activity of some imidazolinone herbicides: a computational approach, *J. Mol. Struct.: THEOCHEM*, 2003, **640**(1–3), 191–200.
94 A. Mahal, M. Al-Janabi, V. Eyüpoğlu, A. Alkhouri, S. Chtita, M. M. Kadhim, A. J. Obaidullah, J. M. Alotaibi, X. Wei and M. R. F. Pratama, Molecular docking, drug-likeness and DFT study of some modified tetrahydrocurcumins as potential anticancer agents, *Saudi Pharm. J.*, 2024, **32**(1), 101889.
95 M. Alcaraz, B. Sharma, F. Roquet-Banères, C. Conde, T. Cochard, F. Biet, V. Kumar and L. Kremer, Designing quinoline-isoniazid hybrids as potent anti-tubercular agents inhibiting mycolic acid biosynthesis, *Eur. J. Med. Chem.*, 2022, **239**, 114531.
96 V. K. Sambandamurthy, S. C. Derrick, T. Hsu, B. Chen, M. H. Larsen, *et al.*, Mycobacterium tuberculosis ΔRD1 ΔpanCD: A safe and limited replicating mutant strain that protects immunocompetent and immunocompromised mice against experimental tuberculosis, *Vaccine*, 2006, **24**(37–39), 6309–6320, DOI: **10.1016/j.vaccine.2006.05.097**.
97 M. D. Johansen, S. Shalini; Kumar, C. Raynaud, D. H. Quan, W. J. Britton, P. M. Hansbro, V. Kumar and L. Kremer, Biological and biochemical evaluation of isatin-isoniazid hybrids as bactericidal candidates against Mycobacterium tuberculosis, *Antimicrob. Agents Chemother.*, 2021, **65**(8), e00011.
98 *S. Schrödinger Release 2021-2: Prime, L.*, New York, NY, 2021.
99 *S. Schrödinger Release 2021-2: Epik, L.*, New York, NY, 2021.
100 *Gaussian 16 Rev. C.01*, Wallingford, CT, 2016.

© 2025 The Author(s). Published by the Royal Society of Chemistry